The Cryogenic AntiCoincidence detector for ATHENA: the progress towards the final pixel design

Claudio Macculi*[a], Luigi Piro[a], Donatella Cea[a], Luca Colasanti[a], Simone Lotti[a], Lorenzo Natalucci[a], Flavio Gatti[b], Daniela Bagliani[b], Michele Biasotti[b], Dario Corsini[b], Giulio Pizzigoni[b], Guido Torrioli[c], Marco Barbera[d], Teresa Mineo[e], Emanuele Perinati[f]
[a]INAF/IAPS Roma, Via del Fosso del Cavaliere 100, 00133 Roma, (Italy)
[b]Dipartimento di Fisica, Università di Genova, Via Dodecaneso 33, 16146 Genova (Italy)
[c]Istituto di Fotonica e Nanotecnologie - CNR, Via Cineto Romano 42, 00156 Roma (Italy)
[d]Dipartimento di Fisica, Università di Palermo, Via Archirafi 36, 90123 Palermo (Italy)
[e]INAF-IASF Palermo, Via Ugo La Malfa 153, 90146 Palermo (Italy)
[f]IAAT-Institut für Astronomie und Astrophysik, Universität Tübingen, 72076 Tübingen (Germany)

ABSTRACT

"The Hot and Energetic Universe" is the scientific theme approved by the ESA SPC for a Large mission to be flown in the next ESA slot (2028th) timeframe. ATHENA is a space mission proposal tailored on this scientific theme. It will be the first X-ray mission able to perform the so-called "Integral field spectroscopy", by coupling a high-resolution spectrometer, the X-ray Integral Field Unit (X-IFU), to a high performance optics so providing detailed images of its field of view (5' in diameter) with an angular resolution of 5" and fine energy-spectra (2.5eV@E<7keV). The X-IFU is a kilo-pixel array based on TES (Transition Edge Sensor) microcalorimeters providing high resolution spectroscopy in the 0.2-12 keV range. Some goals is the detection of faint and diffuse sources as Warm Hot Intergalactic Medium (WHIM) or galaxies outskirts. To reach its challenging scientific aims, it is necessary to shield efficiently the X-IFU instrument against background induced by external particles: the goal is 0.005 cts/cm^2/s/keV. This scientific requirement can be met by using an active Cryogenic AntiCoincidence (CryoAC) detector placed very close to X-IFU (~ 1 mm below). This is shown by our GEANT4 simulation of the expected background at L2 orbit. The CryoAC is a TES based detector as the X-IFU sharing with it thermal and mechanical interfaces, so increasing the Technology Readiness Level (TRL) of the payload. It is a 2x2 array of microcalorimeter detectors made by Silicon absorber (each of about 80 mm^2 and 300 μm thick) and sensed by an Ir TES. This choice shows that it is possible to operate such a detector in the so-called athermal regime which gives a response faster than the X-IFU (< 30 μs), and low energy threshold (above few keV). Our consortium has developed and tested several samples, some of these also featured by the presence of Al-fins to efficiently collect the athermal phonons, and increased x-ray absorber area (up to 1 cm^2).

Here the results of deep test related to one of the last sample produced (namely AC-S5), and steps to reach the final detector design will be discussed.

Keywords: Cryogenic detectors, Anticoincidence, ATHENA, TES

1. INTRODUCTION

ATHENA is a space mission proposal tailored on the scientific theme "The Hot and Energetic Universe"[1] approved by ESA. It will have on-board two instruments: the X-IFU[2] and the WFI[3] (Wide Filed Imager). The instruments are complementary each other: the first will provide detailed image over a small FoV (5' in diameter) featured by very high spectral energy resolution (2.5 eV@E<7keV) so generating for the first time the so-called "Integral field spectroscopy", whereas the second will provide image over a wide FoV (40'x40') but featured by a reduced energy resolution (< 150eV@6keV).

*claudio.macculi@iaps.inaf.it; phone +39 0649934658; www.iaps.inaf.it

One of the X-IFU scientific aim, the reference instrument for our work, it is to provide high spectral energy resolution map of faint or diffuse sources. Hence a very low particle residual background (bkg) around its TES-array detector is necessary, thus an active anticoincidence instrument is necessary to reduce the bkg at the L2 orbit by a factor around one hundred down to the goal of 0.005 cts/cm^2/s/kev[4]. Simple geometric issues shows that this goal is pursued if this anticoincidence is put at a maximum distance of 1 mm below the TES-array, so being a cryogenic detector: the CryoAC. Due to the expected input particle bkg at L2 (~ 3 cts/cm^2/s) it is not necessary to manage the coincidence operation between the CryoAC and the TES-array pulses in real-time on-board the satellite, so sending the data on-ground and performing such an operation off-line (i.e. the CryoAC packet telemetry is low): the CryoAC has an independent electronic chain. A brief overview of the CryoAC program is shown in Ref. 4. The Fig. 1 shows how it is structured the X-IFU instrument: it is shown that the data from the TES-array and the CryoAC independently each other arrive at the ICU (Instrument Control Unit), then to the spacecraft. More details can be found in Ref. 2.

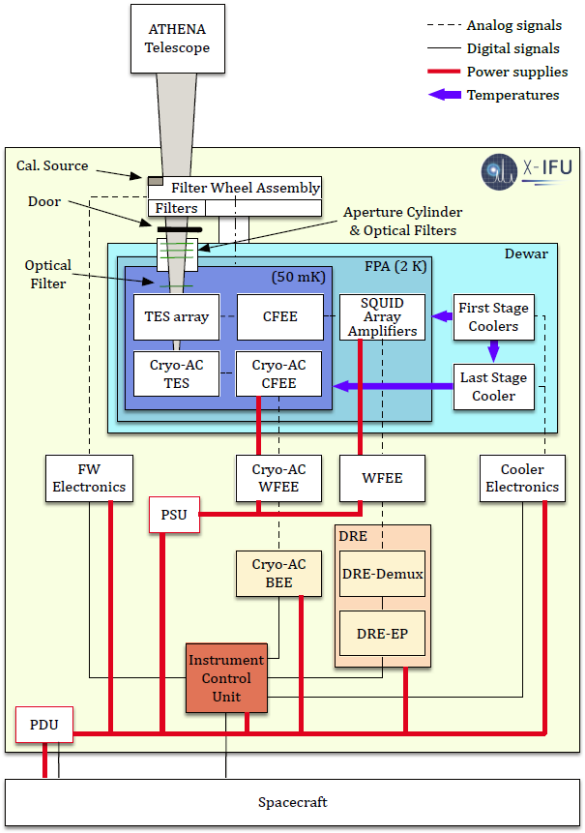

Figure 1. The X-IFU block diagram showing the main system components and the two temperature stages at 50 mK and 2 K. Analog and digital line signals are also shown, together with the power supply lines.

We have designed, produced and tested several CryoAC samples featured by different absorber areas, TES areas and geometries to understand better the physics involved. Results of this scientific path can be found in Ref. 5 and refs. therein.

Here we will present and discuss results related to a deep characterization of one of the last samples so far produced, named AC-S5, which is featured by a high athermal phonons collecting area, i.e. TES-to-absorber ratio area of about 25%. It follows the first characterization we performed on 2012[6]. We remind that the athermal signal generates the prompt used to flag the particles.

This detector, constituted by 2 wide area Iridium TESes deposited on 300 μm thick silicon absorber, it is a quite interesting test-bench to address the path towards the final solution of the CryoAC detector for the ATHENA X-IFU.

As a reference to be compared with the test results the next Table 1 shows the CryoAC main requirements necessary to satisfy the requested scientific performance of the TES-array. Such values are the reference to have a residual particle bkg goal of 0.005 cts/cm^2/s/keV.

Table 1 - CryoAC main requirements.

Parameter	Value
Rise Time constant:	< 30 μs
Decay Time constant:	< 300 μs (Goal)
Bandpass:	20 keV – 0.5 MeV
Area (total, divided on 4 pixels):	~ 4 cm^2

2. THE AC-S5 DETECTOR: BRIEF TECHNICAL OVERVIEW

The main geometrical, and evaluated or measured thermal properties of the AC-S5 detector are shown in Table 2.

Table 2 – AC-S5 main properties. About the TES thermal capacitance we insert the "expected" normal-metal value.

Parameter	Value
Absorber Silicon Area:	6x7 mm^2
Absorber Silicon Thickness:	300 μm
TES Area:	2x(2x5) mm^2
TES thickness:	300 nm
C_{Si}:	6.7 pJ/K (at 0.105 K)
C_{TES}:	2*130 pJ/K (at 0.105 K)
T_C:	~ 105 mK
ΔT_C:	~ 10 mK
R_N (1 TES):	~ 0.150 Ω
R_N (2 TES in parallel configuration):	~ 0.120 Ω
α_{max}:	~ 50
Collecting Area (TES/Absorber):	24%

Note that about the TES thermal capacitance we insert the "expected" normal-metal value. From the BCS theory it is expected that the effective working value can increase up to 2.43 time this one depending on the working point along the transition. Since no impedance measurement setup has been implemented up to now we get as a reference value the average inside this range, roughly 220 pJ/K per each TES. A picture of AC-S5 is shown in Fig. 2. The two TESes are clearly visible.

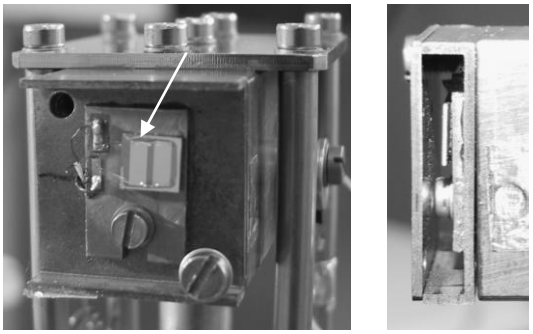

Figure 2. The AC-S5 detector mounted on the sample holder (Copper). Hereafter TES1 is the first on the left (see the arrow). On the right it is shown its lateral side: the radioactive source will be located in front of the detector in contact with the Cu frame (not visible in this figure).

The sample has been tested before with one TES (i.e. TES1, the first on the left of Fig. 2), and then with both the TESes. This procedure has been done to better understand how the microcalorimeters works in collecting the athermal phonons.

3. THE AC-S5 DETECTOR WORKING WITH THE TES1

We have characterized the detector by standard measurements to know its transition, and from the I-V curve to evaluate the thermal conductance to the thermal bath. The results are reported in Figg. 3 (left) and 4. We have also measured the input inductance (Fig. 3 right) when the TES was fully superconductive, which is due to the SQuID input coil (Lin ~ 6 nH) plus parasitic (stray) one: the sum is about 267 nH mainly due to the long wiring (Nb/Ti-Cu/Ni matrix) from the TES to the SQuID located at ~ 3K. This value is important to assess the pulses rise time constant. We remark that the adopted SQuID is the 16-SQUID series array (type C6X216FB) from Magnicon.

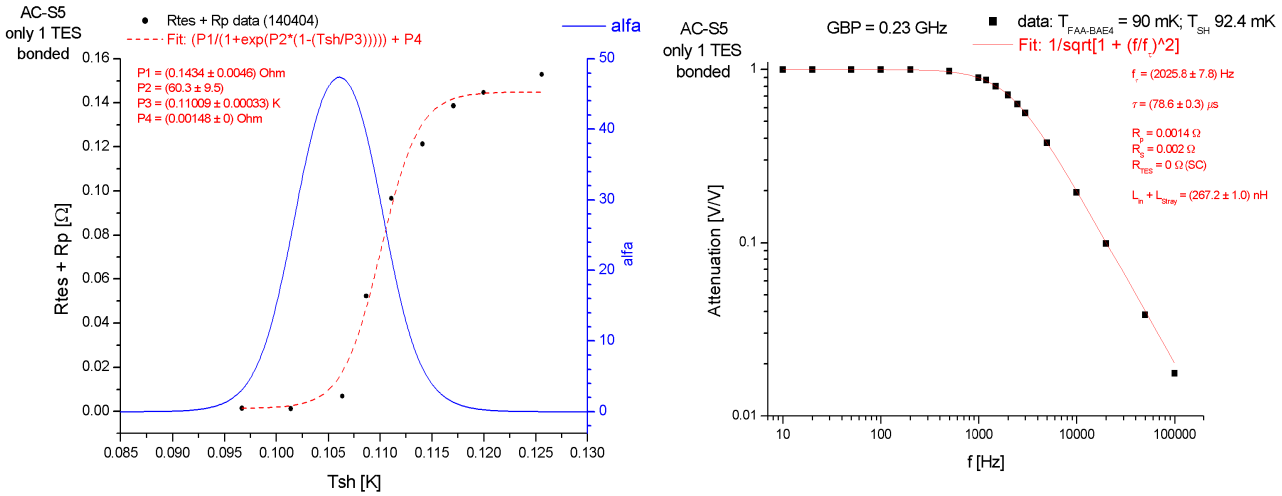

Figure 3. (left) Transition measurement for TES1. (right) Evaluation of the total input inductance of the input circuit.

The transition starts at about 105 mK and it is ~ 0.150 Ω. To get the α value we have performed a fit on the transition data and then computed the values.

About the thermal conductance, it has been evaluated by a simple linear model (Fig. 4) as also shown in the inset by a roughly constant value of the power derivative: G ~ 2E-8 W/K. This analysis is indeed justified since the thermal bath temperature is closed to the critical temperature, and the linear model also provides a critical temperature of T_C ~ 0.105 K fully compatible with the transition temperature.

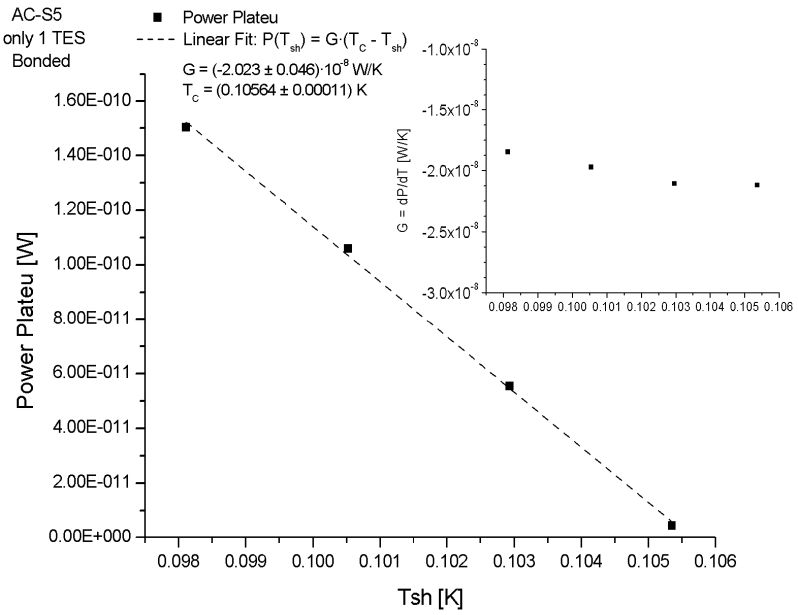

Figure 4. Power plateau vs sample holder temperature. The inset shows the thermal conductance to the thermal bath.

Hence, by taking into account the adopted value of ~ 220 pJ/K for each TES thermal capacitance, we expect a AC-S5 microcalorimeter thermal decay time constant of about 22 ms.

3.1 The pulses raw analysis

The detector has been illuminated by means of a shielded (0.5 mm Cu thick) ^{241}Am source, so only the 60 keV line is expected for the acquisition time duration. The ADC has been set at 2MS/s, and all the data have been both amplified (G = 200 V/V) and filtered (Stanford SR560) by a lowpass 1-pole at 10kHz due to the high level of noise present, so defining a filtering time constant of about 15 us. The detector has been polarized by Ib = 600 μA, that provides a TES polarization current of Ites = 39 μA, Rtes ~ 0.03 Ω, Vtes ~ 1.12 μV, Ptes ~ 44 pW, Ttes ~ 0.107 K. By taking into account a shunt resistance of the Magnicon SQuID of about 2 mΩ, we get a loop gain L = 0.9. Hence the expected ETF-thermal decay time constant is ~ 12 ms, and the fastest electronic time constant is ~ 10 μs, but due to the LP filtering, about 15 μs is then expected for the pulses rise time constant.

The following data analysis is referred to pulses acquired by a software trigger. Then, since they were affected by EMI noise in the interesting frequency band, a preliminary analysis to extract pulses from unlocking signals or also spikes has been performed. Some pulses after this preliminary analysis are shown in Fig. 5.

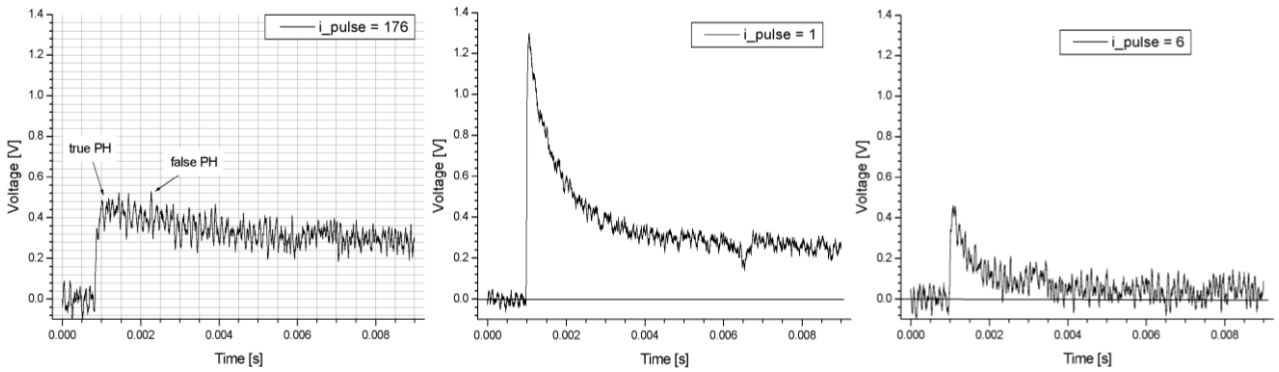

Figure 5. AC-S5 TES1: examples of triggered pulses. It is evident the in-band EMI (see text for details).

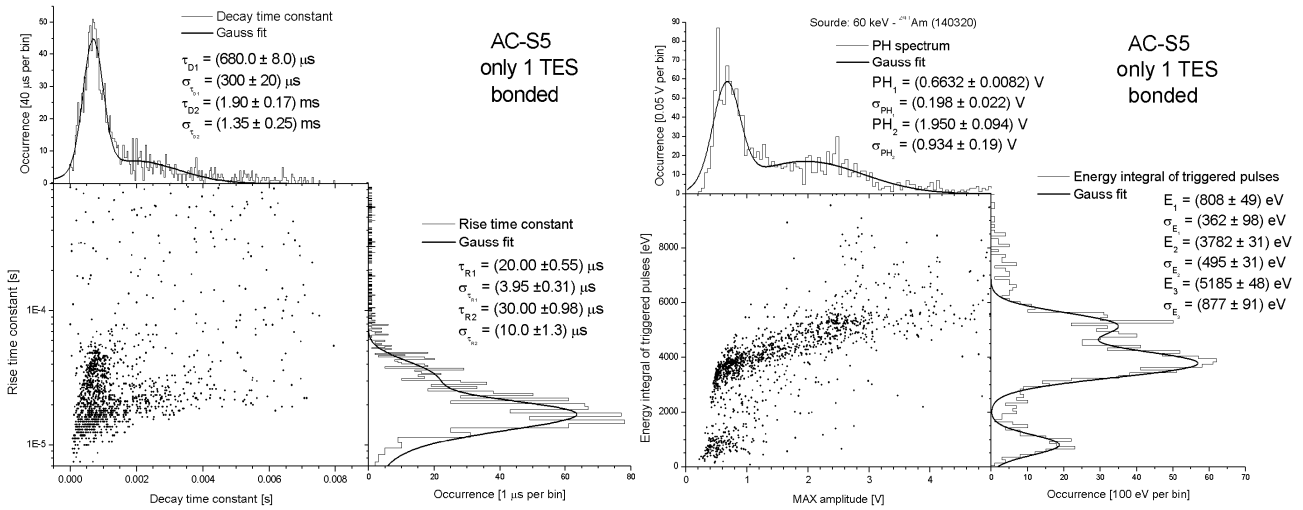

Figure 6. (left) Rise time vs Decay time constants from raw analysis. (right) Energy integral of the triggered pulses vs their PH.

A very raw analysis has been performed on the pulses to know their timings and spectrum. The timing results are shown in Fig. 6-left. The time constants have been here roughly evaluated by taking into account as reference the maximum value of the recorded data for each pulse. The rise time constant is well defined around the value of τ_R = (20.00 ± 3.95) μs fully compatible with the LP filtering, as expected, and a decay time constant of τ_D ~ 680 μs. At the moment no athermal model has been produced to know what is the expected value, but we see that in this working point the microcalorimeter has the rise time inside the requirement and the decay time about a factor two slower with respect to what required (see Table. 1). Note that the decay time here reported is quite different from the expected value of ~ 12 ms because the latter is due to the thermal component. We have also highlighted a second "bump" but, as shown later, such values are probably due to EMI (~ 7 kHz) that affects the measurement, then this raw analysis: from the Fig. 5 the first pulse on the left shows the case where the maximum value of the pulse (indicated as "false PH") is considered as true by this raw analysis but it occurs later than the "true PH", so providing both a longer rise and decay time constants. The problem is related to in-band (~ 7 kHz) spurious frequencies.

The spectrum (Fig. 6 - right) highlights the presence of the athermals, and provides several features. Later we will discuss these results that will be more clear when compared with to the ^{55}Fe spectrum but, roughly, it strongly depends on the athermals collecting efficiency. A rough evaluation of the energy resolution evaluated by the second peak ($2.35 \cdot \sigma_{E2}/E2$) provides a value of about 30%. From the PH spectrum we get ~ 70 % (to be compared with the result in section 4).

3.2 The double pulse fitting analysis for the TES1 case

The double-pulse fitting procedure will help in solving several issues because it disentangles the athermal component from the thermal one. An example of the fitting is shown in Fig. 7.

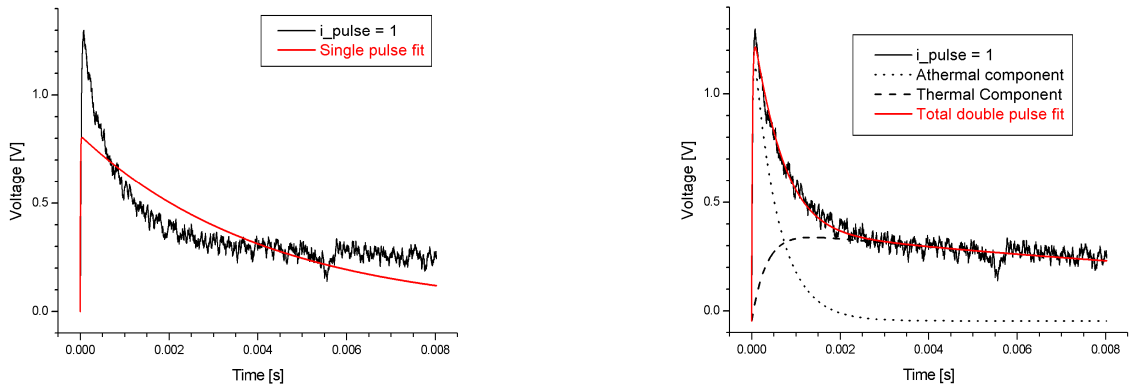

Figure 7. Fitting procedure over the triggered pulses: on the left single pulse, on the right double pulse which disentangles the athermal from the thermal component.

The next Fig. 8 shows the PH spectra to understand the athermals collection with respect to the thermals, so how the detector works in different regimes.

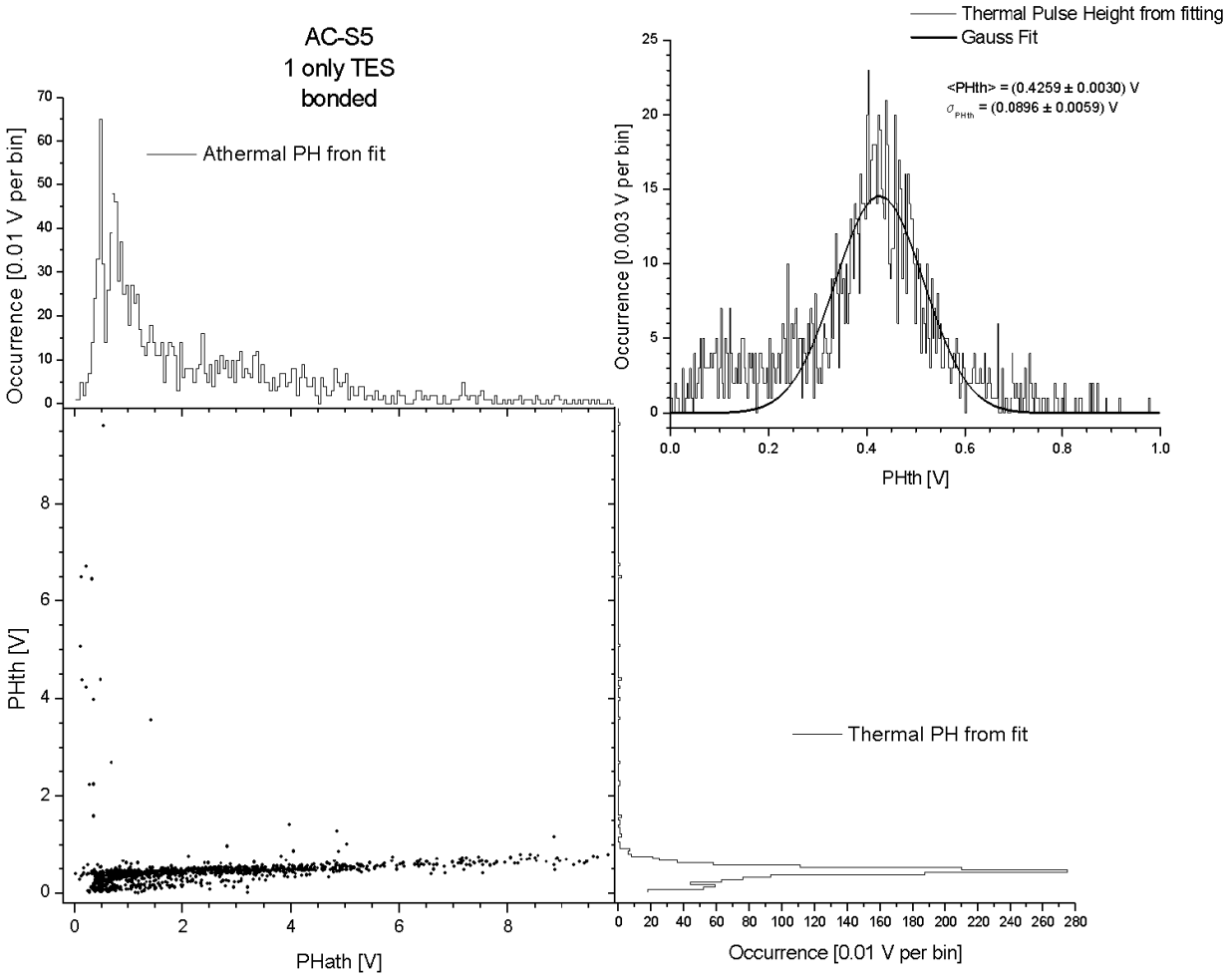

Figure 8. PH spectra from the double pulse fitting procedure: Thermal vs Athermal. The inset show details on the thermal spectrum highlighting a well shape line at 60 keV around 0.43 V.

The spectra are plotted on the same scale to appreciate the different regime: from the thermal point of view the detector shows a more spectroscopic capability with respect to the athermal regime. Keep in mind that at the moment only TES1 is active, in the next section we will show the trend by operating the detector with both the TES. The inset shows details about the thermal spectrum: the bump on the left (here not fitted) is visible only by the thermals and, as shown later, it is an evidence of the copper fluorescences.

The athermal decay time constant vs thermal decay time constant is shown in Fig. 9. It is worth of note that the gaussian fit over the thermal component provides a central value of 12 ms, fully compatible with what expected from previous assessment (section 3.1). Here it is not reported but the thermal rise time constant is similar to the athermal decay time since the thermal phonon family is populated when the athermals decay, and this trend has been seen in several experiments[7, 8].

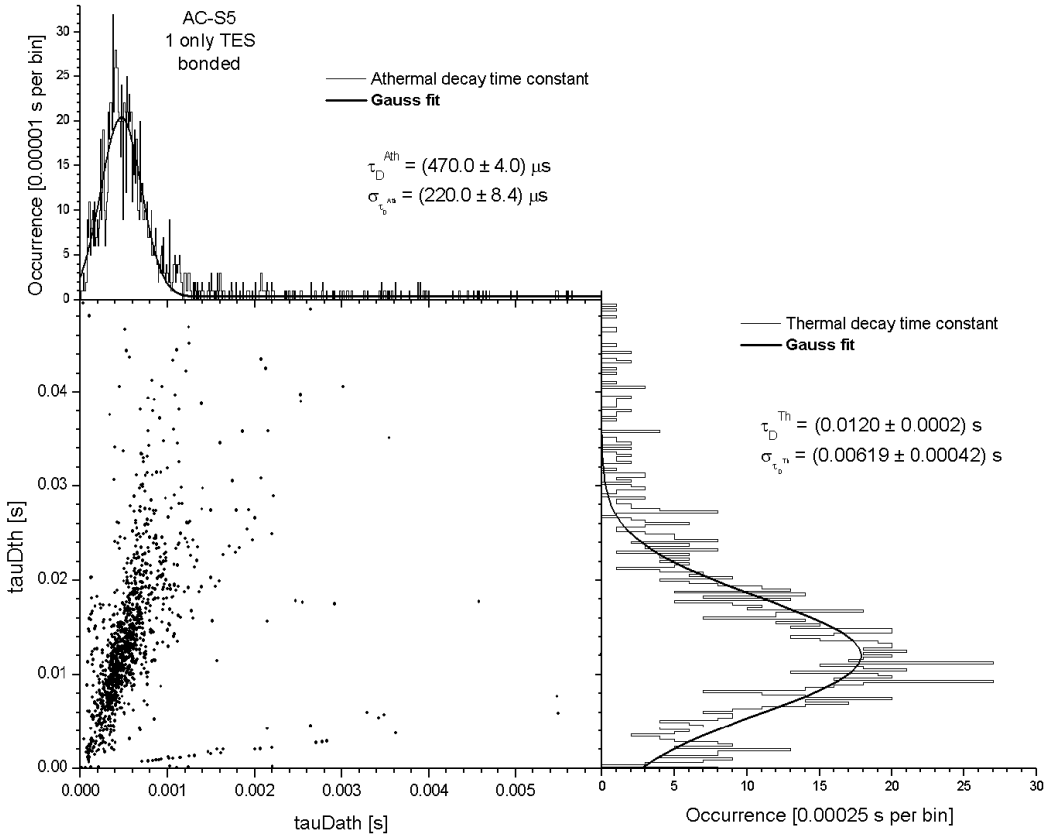

Figure 9. Athermal decay time constant vs thermal decay time constant. The central value of the tauDth distribution is fully compatible with what expected.

The detector has been also illuminated by the ^{55}Fe55 source, and the energy spectrum evaluated by the in-time integral of the triggered pulses is shown in Fig. 10. To better understand the spectrum it is useful to know where both the photons of the ^{55}Fe and of the ^{241}Am (60 keV) are expected to be absorbed.

At 6 keV (^{55}Fe) the transmission in silicon diminishes to the value "1/e" at the thickness d ~ 30 μm. At 60 keV, the transmission is attenuated in silicon to the value "1/e" at d ~ 14400 μm. Since the thickness of the AC-S5 Silicon absorber is 300 μm, this implies that the majority of the events of ^{55}Fe are absorbed to about 1/10 of its thickness, then at the "surface" level, instead at 60 keV photons must cross the whole material to increase the absorption probability (at 60 keV and 300 μm thick, the Silicon absorption efficiency is 0.02). Hence, the ^{241}Am events affect the entire volume. Therefore the Iron source generates phonons much more close to the TES than those generated by the Americium.

Despite the Americium generates approximately 10 times more phonons of Iron (60 keV at 6 keV), so more carriers, in fact the Iron photons are immediately seen by TES, those from the Americium generated in depth have longer path to reach the TES and, since the first generated signal is the Athermal it is intuitive that many will be lost if not well collected. Therefore, the response of the microcalorimeter to 60 keV should be more deformed if compared to the 6 keV, as observed in the spectrum. The next plot shows this situation, and it is also interesting because provides the evidence of the copper fluorescences produced by the Americium through the setup (see Fig. 2 for details), so possibly moving the effective energy threshold lower than 10 keV, better than the requirements.

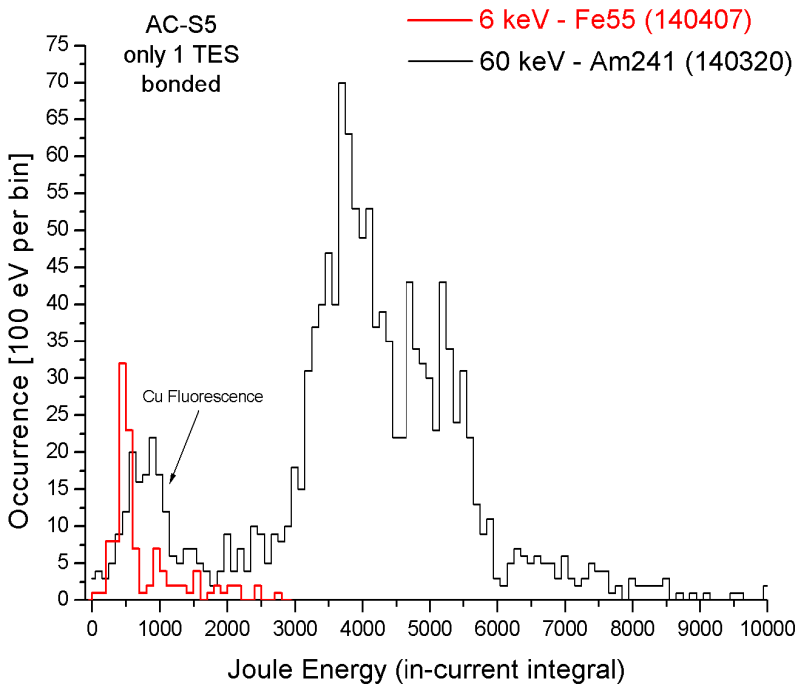

Figure 10. Comparison between the ^{55}Fe and the ^{241}Am (60 keV): the Cu fluorescences is evident. The energy integral comes from the in-current integral of the triggered pulses.

We conclude this section providing some information about the amount of the deposited energy with respect to the input. The two main ingredients that affect the effective energy computed by the pulse integral are the loop gain of the TES working point and, in our case, also the athermal collection efficiency which is also the "prompt" that drives the thermal signal. By collecting information from several papers[9, 10, 11], the measured energy can be roughly represented as,

$$E_{\text{measured}} = \left(\frac{L}{L+1}\right) \cdot E_d = \left(\frac{L}{L+1}\right) \cdot \varepsilon_{ph \to TES} \cdot E_\gamma \qquad (1)$$

where L is the loop gain, E_d the deposited energy "sensed" by the TES, $\varepsilon_{ph \to TES}$ is the efficiency of reading the phonon signal in the TES (this parameter takes into account the phonon collecting efficiency and the amount of the input energy that goes in phonons), and E_γ the input energy. It is also expected that the energy resolution is worsened by the factor $\varepsilon_{ph \to TES}$ (not full energy collection, then $\Delta E_{eff} = \Delta E_{fwhm} / \varepsilon_{ph \to TES}$), so an estimate of this factor could be derived by the ratio between the 1-sigma baseline noise (Fig. 11), that should be close to the expected energy resolution, and the 1-sigma spread of the thermal spectrum.

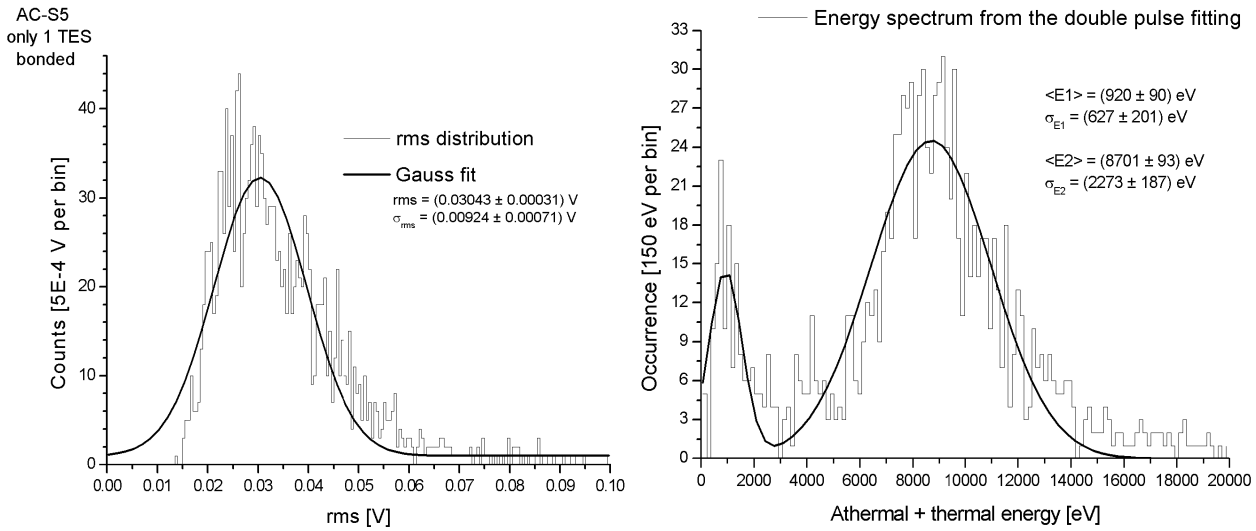

Figure 11. (left) rms noise distribution from the pulses baseline. (right) Full spectrum computed by the double pulse fit.

From Fig. 8 we get σ_E ~ 0.09 V, and since rms ~ 0.03 V (Fig. 11 -left), then $\varepsilon_{ph \to TES}$ ~ 0.3. Hence, since L ~ 1, we expect about 15% of energy measured by the detector, that for the 60 keV means about 9 keV, and the copper fluorescences around the 8 keV K_α is expected at ~ 1 keV, as shown by the right plot of Fig. 11.
It is worth of note that the energy spectrum in Fig. 11 right is different with respect to the one in Fig. 10 since in Fig. 11 the energy is computed by taking into account the parameters extracted from the fitting, i.e. " PH*(τ_D - τ_R)" so taking into account all the expected pulse duration, instead in Fig. 10 the integral to get the energy is performed on the triggered pulses that, as shown in Fig. 5, were truncated during the acquisition.

4. THE AC-S5 DETECTOR WORKING WITH BOTH THE TES

We report in Fig. 12 the transition measurement and the thermal conductance towards the bath extracted from the I-V curve. After two years the transition measurement provides compatible results with the previous one. It is a quite important results since it shows that both the TES manufacturing process and the used material (Iridium deposited onto the Silicon substrate) are reliable.

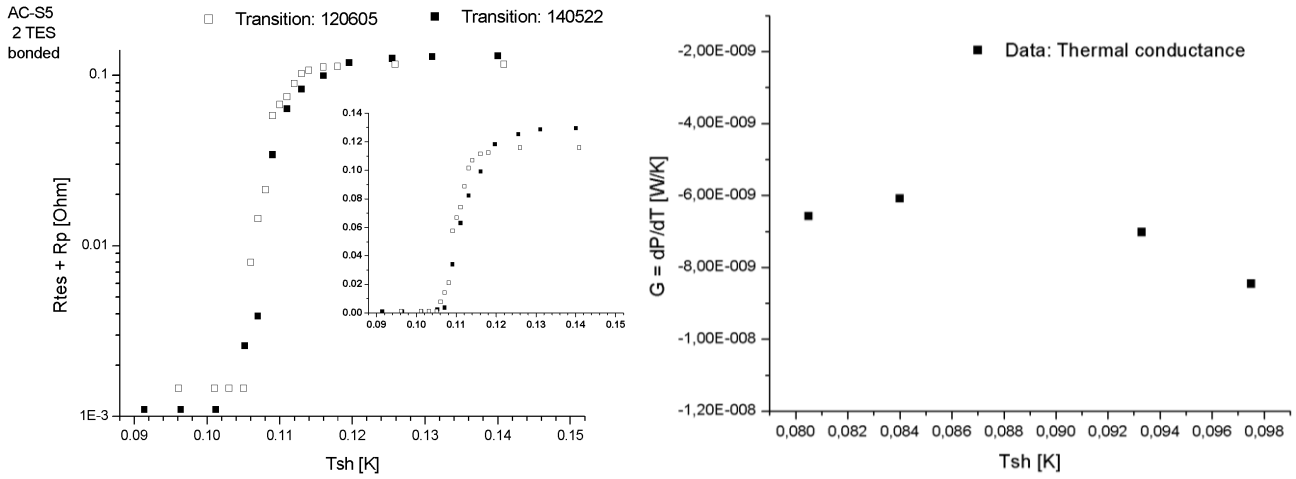

Figure 12. (left) Comparison between the transition measurement done after a two years time period. (right) – Thermal conductance evaluated from the I-V curve

The thermal conductance provides the value of 6E-9 W/K at Tsh = 84 mK, which is the temperature working point where the microcalorimeter has been operated by illuminating it with the 60 keV line of ^{241}Am.
The ADC to acquire pulses has been set at 2MS/s, and all the data have been both amplified (G = 20 V/V) and filtered (Stanford SR560) by a lowpass 1-pole at 10kHz due to the high level of noise present, so defining a filtering time constant of about 15 μs. The acquisition time has been doubled with respect to the TES1 case. The detector has been polarized by Ib = 700 μA, that provides a TES polarization current of Ites = 90 μA, Rtes ~ 0.014 Ω, Vtes ~ 1.22 μV, Ptes ~ 110 pW, Ttes ~ 0.105 K, alfa = 27. By taking into account a shunt resistance of the Magnicon SQuID of about 2 mΩ, we get a loop gain L = 3.5. Hence the expected ETF-thermal decay time constant is ~ 17 ms. Since the electronic time constant from the input circuit is L/R ~ 20 μs and the LP filtering is about 15 us, it is then expected for the pulses rise time constant a value around 15-20 μs.
The next Fig. 13 reports the results from the raw analysis performed on the triggered pulses.

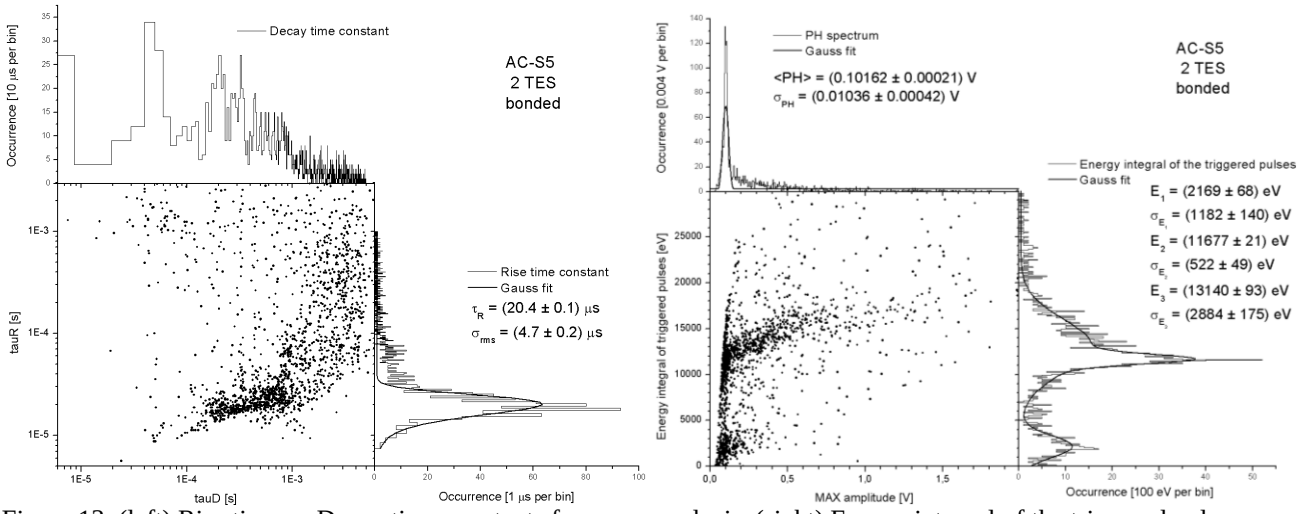

Figure 13. (left) Rise time vs Decay time constants from raw analysis. (right) Energy integral of the triggered pulses vs their PH.

The rise time constant is compatible with the expected value and the decay time constants roll by the range 0.1-1 ms. Quite interesting is the plot on the right that shows Energy integral of the triggered pulses vs their PH to be compared with the one in Fig. 6 (right): the 2-TES case provides a more narrow line with respect to the TES1 case, showing that the increase of athermals collecting efficiency improves the spectrum. A rough evaluation of the energy resolution evaluated by the second peak ($2.35 \cdot \sigma_{E2}/E2$) provides a value of 10% to be compared with the 30% from the TES1-case (Fig. 6-rigth). From the PH spectrum we get ~ 24 %, to be compared with the 70% from the TES1-case: an improvement by a factor ~ 3.

4.1 The double pulse fitting analysis for the 2 TESes case

By taking into account the microcalorimeter working point, it is expected 17 ms as ETF-thermal decay time constant, roughly consistent with the results (Fig. 14 - left). The athermal decay time constant is around 450 μs. Both the Athermal and the Thermal PH spectrum are well shaped (Fig. 14 - right).

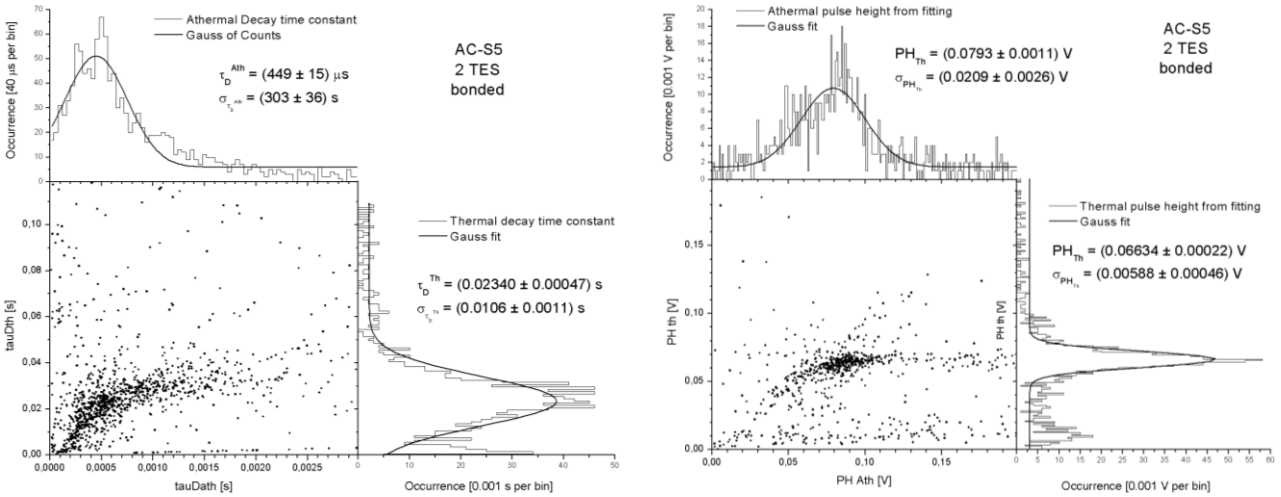

Figure 14. (left) ETF thermal decay time constant vs athermal decay time constant. (right) Thermal PH spectrum vs the Athermal PH one. About the thermals only the gauss fit on the 60keV line is shown.

We conclude this section providing the Energy spectrum evaluated by the results from the double pulse fitting procedure.

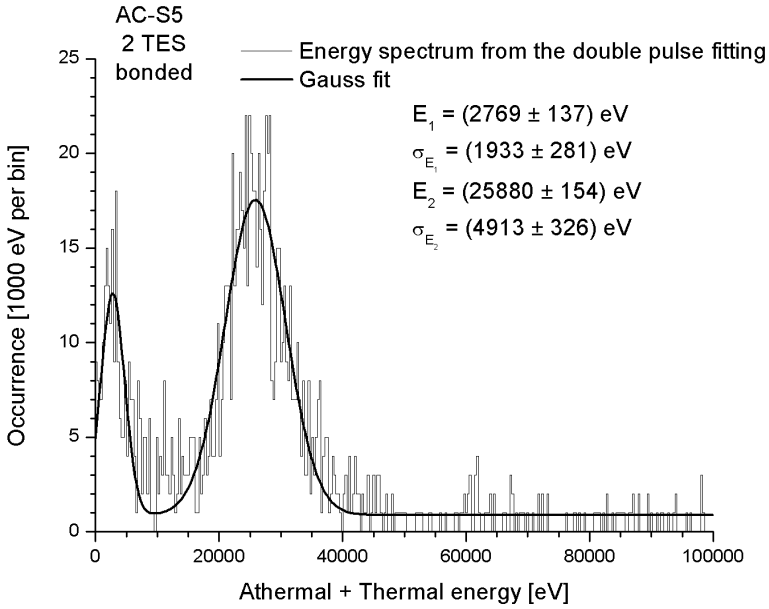

Figure 15. Total energy sensed by the 2 TESes evaluated from the double pulse fitting procedure.

By taking into account the peak at 26 keV and the loop gain L = 3.5, from Eq. 1 it is possible to evaluate the "efficiency of reading the phonon signal in the TES" parameter as $\varepsilon_{ph \to TES}$ ~ 0.6 which is twice the value of TES1, as expected since in this case the TES coverage area is doubled, so also the athermal collecting efficiency. Further, the main peak is located at an energy which is a factor 3 greater than the TES1 case, so scaling as expected due both to the loop gain L and $\varepsilon_{ph \to TES}$. Lastly, as for the TES1 case, the Copper fluorescences expected here around 3 keV are evident.

This result improves the consistency of the analysis, so all the evaluations here reported.

5. CONCLUSIONS

In this work we have reported a deep investigation of the AC-S5 prototype which is a quite interesting detector since, being featured by 2 wide TES, it can provide information on how the microcalorimeter works in collecting the athermal phonons that "form" the flags to veto the particles hits onto the X-IFU TES-array.

This prototype provides most of the parameter inside the requirements: τ_R ~ 20 μs (< 30 μs from the REQs.), threshold about 10 keV highlighted by the presence of the Copper fluorescences (20 keV from the REQs.), τ_D ~ 500 us which is roughly a factor 2 greater than the value from the REQs (300 μs). The area is a factor 2 smaller than the baseline one of about 0.81 cm^2 (array of 4 pixels).

It is clear how the deposited energy is lower than the input energy. As shown from the Eq. 1, the "collected" energy depends on both the loop gain L and the $\varepsilon_{ph\to TES}$ parameters. From our results, the parameter $\varepsilon_{ph\to TES}$ which is the "efficiency of reading the phonon signal in the TES" scales as the TES area-to-Absorber area ratio: it is a quite important result because we have for the first time the evidence on how to quantify the athermals collecting efficiency and their effects on the measured energy. In detail, double the TES area (from 1 TES to 2 TESes) then the athermal collecting efficiency, $\varepsilon_{ph\to TES}$ is doubled moving from ~ 30% to ~ 60%. By taking into account also the loop gains for both the tests, we see that the measured energy for the 2-TES run has increased by a factor 3 from TES1 as expected: this is a clear evidence on how both the L and the $\varepsilon_{ph\to TES}$ parameters work.

By using the results from the raw analysis, the increase of the athermal collecting efficiency improves also the energy resolution of the detector related to the PH spectra: moving from the TES1 case to the 2-TES one we get an improvement of about a factor 3.

In conclusion, these results not only provides strong hints on how to design the CryoAC towards the flight configuration, but also put a strong jump on the TRL, so having now a TRL very close to 4.

ACKNOWLEDGEMENT

We acknowledge both the IAPS institute for having provided resources to continue this activity and Didier Barret for useful comments.

REFERENCES

[1] Nandra, K., Barret, D., Barcons, X., Fabian, A., den Herder, J.-W., Piro, L., Watson, M., Adami, C., Aird, J., Afonso, J. M., and et al., "The Hot and Energetic Universe: A White Paper presenting the science theme motivating the Athena+ mission," 2013arXiv1306.2307N (2013).

[2] Ravera, L., Barret, D., den Herder, Jan-Willem, Piro, L., et al, "The X-ray Integral Field Unit (X-IFU) for Athena", in this proceeding, paper 9144–92 (2014).

[3] Rau, A., Meidinger, N., Nandra, K., et al, "The Hot and Energetic Universe: The Wide Field Imager (WFI) for Athena+", 2013arXiv1308.6785, (2013)

[4] Lotti, S., Perinati, E., Natalucci, L., Piro, L., Mineo, T., Colasanti, L., Macculi, C., Federici, M., Martino, B., "An efficient method for reducing the background of microcalorimeters applied to ATHENA-XMS", Proc. of SPIE, Vol. 8443 84435H-1, (2012).

[5] Macculi, C., Piro, L., Colasanti, L., Lotti, S., Natalucci, L., Bagliani, D., Biasotti, M., Gatti, F., Torrioli, G., Barbera, M., Mineo, T., Perinati, E., "The Cryogenic AntiCoincidence Detector Project for ATHENA+: An

Overview Up to the Present Status", Journal of Low Temperature Physics, DOI:10.1007/s10909-014-1150-4 (2014).
[6] Macculi, C.; Piro, L.; Colasanti, L.; Lotti, S.; Natalucci, L.; Bagliani, D.; Biasotti, M.; Gatti, F.; Torrioli, G.; Chiarucci, S.; Barbera, M.; Mineo, T.; Perinati, E., "The cryogenic anticoincidence detector for ATHENA-XMS: preliminary results from the new prototype", Proc. of SPIE, Vol. 8443, 84435G, (2012).
[7] Westphal, W., "Development and Characterization of Cryogenic Detectors for the CRESST Experiment", PhD thesis, Technische Universitat Munchen, (2008).
[8] Macculi, C., Colasanti, L., Lotti S., Natalucci, L., Piro, L., Bagliani, D., Biasotti M., Gatti, F., Torrioli G., Barbera, M., La Rosa, G., Mineo, T., Perinati, E., "The Cryogenic Anticoincidence Detector for ATHENA-XMS", JLTP, 167, 783-794, (2012)
[9] Figueroa-Feliciano, E., "Theory and development of position-sensitive quantum calorimeters", PhD thesis, Stanford, (2001)
[10] Miller, A. J., "Development of a broadband optical spectrophotometer using superconducting Transition Edge Sensors", PhD thesis, Stanford, (2001)
[11] Leman, S.W., Figueroa-Feliciano, E., Kilbourne, C.A., T. Saab, T., "Cryogenic Hard X-ray Imaging Spectrometer for the International X-ray Observatory", Procceding of LTD13, AIP Conf. Proc. 1185, 703 (2009).